Infante-García, D.; Giner Maravilla, E.; Miguélez, MH.; Wahab, MA. (2019). Numerical analysis of the influence of micro-voids on fretting fatigue crack initiation lifetime. Tribology International. 135:121-129. https://doi.org/10.1016/j.triboint.2019.02.032

# Numerical analysis of the influence of micro-voids on fretting fatigue crack initiation lifetime

Diego Infante-García[1], Eugenio Giner[2], Henar Miguélez[1], Magd Abdel Wahab[3,4*]

[1] Department of Mechanical Engineering. Universidad Carlos III de Madrid, Avda. de la Universidad 30, 28911 Leganés, Madrid, Spain

[2] Centre of Research in Mechanical Engineering – CIIM, Department of Mechanical and Materials Engineering, Universitat Politècnica de València. Camino de Vera, 46022 Valencia, Spain

[3] Institute of Research and Development, Duy Tan University, 03 Quang Trung, Da Nang, Viet Nam

[4] Soete Laboratory, Faculty of Engineering and Architecture, Ghent University, Technologiepark Zwijnaarde 903, B-9052 Zwijnaarde, Belgium

*Corresponding author: magd.abdelwahab@ugent.be

## Abstract

In this paper, the influence of the heterogeneity in the predicted crack initiation lifetime under fretting fatigue conditions is analysed for a regular and a random distribution of micro-voids. A critical plane analysis with two multiaxial damage criteria is performed to assess the crack initiation lifetime. The predicted initiation lifetime in the heterogeneous material is compared with the results obtained in the homogeneous case. The numerical results show that the heterogeneity has a noticeable influence on the predicted initiation lifetime. Furthermore, the numerical model suggests that a crack may firstly initiate at the upper edge of the micro-voids located close to the contact edge. generally leading to a mean reduction of the predicted crack initiation lifetime. However, in some cases, the introduction of micro-voids reduces the stress intensity at the contact edge and, so decreasing the predicted crack initiation lifetime.

## Keywords

Heterogeneous material, Fretting fatigue, Finite element method, Prediction crack initiation

## 1. Introduction

Fretting happens when two or more solids are in contact with some minute relative displacement [1]. In addition, lifetime of components under fretting conditions is usually reduced compared to plain fatigue conditions [2], leading to the failure of many engineering components [3]. Thus, prediction of fretting fatigue lifetime has a great demand from industry and damage tolerance design approaches. Prediction models should consider the non-proportionality stress state and severe stress gradients that are present in components subjected to fretting fatigue. In addition, numerical methodologies found in the literature usually consider the material as perfectly homogeneous [2,4–12]. However, metals may present some degree of micro-porosity or defects due to manufacturing as in casting or metal additive manufacturing [13,14]. On the other hand, thermal spray coatings are usually employed to increase the fretting strength of a component, although in some cases they may generate some micro-voids on superficial layers [15]. In this way, the influence of the heterogeneity should be taken into account for accurate prediction when using numerical methodologies [16].

The damage process of fretting fatigue can be classified into two stages [17]: stage I for the crack initiation process and stage II for the crack propagation process. Stage I is usually dominated by the shear stress range (type I crack in stage I) according to Dubourg et al. [18] although in some cases cracks can be dominated by the normal stress range (type 2 crack in stage I). Once the crack has reached some critical length, the crack escapes from the influence of the contact and starts to be dominated by the cyclic axial load (transition stage I/II), kinking to the maximum normal stress range.

The lifetime estimation of crack initiation and crack propagation is usually calculated separately due to damage process classification (stage I and stage II) [12]. Several damage models and approaches can be found in the literature for the lifetime estimation through

crack initiation. Following the review of Bhatti and Wahab [19], these methodologies can be classified into: critical plane analysis, stress invariant approaches, fretting specific parameters and continuum damage mechanics.

On the other hand, lifetime estimation through propagation models of an initial crack or flaw is usually assessed through linear elastic fracture mechanics (LEFM) and finite element models (FEM) [6,11]. A few parameters need to be defined such as size, location and orientation of the initial crack or flaw. Experimental results have shown that cracks usually grow pointing to beneath the contact zone [20–22]. Furthermore, a crack orientation criterion for non-proportional loading is necessary to assess the crack path [22]. Generally, crack propagation lifetime is assessed through stress intensity factors calculation along the crack path and by the application of a fatigue crack growth law, such as the Paris law [6].

Few studies have been found regarding the influence of heterogeneity in the fretting fatigue behaviour. Kumar et al. [23] analysed numerically the influence of heterogeneity in the stress state under fretting conditions through Direct Numerical Simulations (DNS). They conclude that the heterogeneity has a relevant effect in the shear stress state, being more critical than the homogeneous case. Erena et al. [24] studied numerically the influence of the introduction of voids in plain fretting on the damage severity using a critical plane approach and a multiaxial damage criterion. The authors showed a decrease in the damage parameter for certain configurations of the micro-voids and suggest its employment as a palliative. On the other hand, metals with some degree of porosity or defects have shown that crack initiation is usually located on the surface or at the vicinity of porous or defects located close to the surface of the component [25,26]. Therefore, the crack initiation and propagation stages may be significantly affected under fretting fatigue as well. In addition, initial crack location and orientation may be also influenced due to

the presence of micro-voids.

In this paper, the effect of heterogeneity has been analysed numerically using DNS on the crack initiation lifetime under fretting conditions. The heterogeneity has been included as micro-voids in the specimen. The shape of micro-voids is simplified to a circle. Two micro-void distributions are considered: regular and random distributions. A critical plane analysis in combination with the Theory of Critical Distances [27] (TCD) is performed to predict the crack initiation. The analysis is also performed considering the material as homogeneous to assess the influence of the heterogeneity on the predicted results.

## 2. Materials and methods

### 2.1. Experimental data and materials

The experimental fretting fatigue test published by Hojjati-Talemi et al. [7] is taken as reference. The test set-up consists in a cylinder-to-plane contact configuration under constant normal load ($P$) (see Fig. 1). Two cylinders of 50 mm radius are symmetrically clamped to a dog bone specimen, both made of AL2024-T3. The specimen is subjected to a cyclic axial load ($\sigma_{axial}$) and the pads are fixed with leaf springs to the platform, given rise to a cyclic tangential force ($Q$) between both components (further details about the test set-up can be found in [7]).

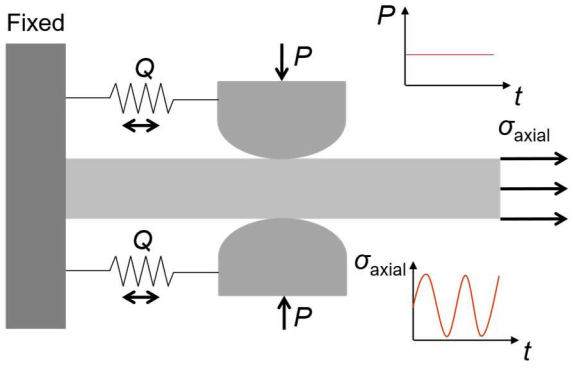

Figure 1: Sketch of the test configuration.

The Young's modulus (*E),* Poisson's ratio ($\nu$), yield strength ($\sigma_y$) and ultimate strength ($\sigma_u$) of AL2024-T3 are given in Table 1 [7]. The stress ratio of $\sigma_{axial}$ and $Q$ is 0.1 and -1, respectively.

| 2024-T3 | $\sigma_y$ [MPa] | $\sigma_u$ [MPa] | $E$ [GPa] | $\nu$ [-] |
|---|---|---|---|---|
| | 383 | 506 | 72.1 | 0.33 |

Table 1: Mechanical properties of 2024-T3 [7].

The coefficient of friction (COF) between pad and indenter was measured by Hojjati-Talemi et al. [7] under partial slip conditions giving a value of 0.65. Hojjati-Talemi et al. [7]. The methodology proposed by Araújo and Nowell in [28] allowed for the measurement of the steady COF under partial slip conditions (after $10^3$ cycles) using the Digital Image Correlation technique. The total number of cycles ($N_f$) until complete fracture was recorded by Hojjati-Talemi et al. [7] for each test condition. The value of the normal load is kept constant for all the test conditions, being equal to 135.75 N/mm. The total lifetime for the nine conditions tested is reported in Table 2.

| Test condition | $\sigma_{axial}$ [MPa] | $Q_{max}$ [N/mm] | $N_f$ [cycles] |
|---|---|---|---|
| 1 | 100 | 38.79 | 1407257 |
| 2 | 115 | 46.56 | 1105245 |
| 3 | 135 | 55.93 | 358082 |
| 4 | 135 | 48.89 | 419919 |
| 5 | 160 | 48.43 | 245690 |
| 6 | 190 | 82.54 | 141890 |

| | | | |
|---|---|---|---|
| 7 | 205 | 80.53 | 114645 |
| 8 | 220 | 66.79 | 99607 |
| 9 | 220 | 79.46 | 86647 |

Table 2: Cycles to fracture for the tests carried out by Hojjati-Talemi et al. [7] (maximum value of the cyclic axial load is reported).

### 2.2. Numerical model for crack initiation

The finite element (FE) software Abaqus Standard © has been employed to obtain the stress field under fretting conditions. Inertial effects are not considered so a quasi-static problem has been analysed. The material has been considered purely elastic (maximum principal stresses are below the yield strength in all cases). The tangential load has been introduced through the definition of the cyclic reaction load ($\sigma_{react}$) on the other edge of the specimen as sketched in Fig. 2. The methodology is analogous as in [6,7,23]. Half of the specimen has been modelled in 2D due to symmetry conditions. The augmented Lagrange multipliers method has been employed to model the friction with a master-slave approach. The Multi Point Constraint (MPC) is applied on the top edge of the indenter to avoid rotations. Both sides of the indenter and bottom of the specimen are restricted in the *x* direction and *y* direction, respectively. Boundary conditions are also detailed in Fig. 2 for the sake of clarity. Plane strain condition is assumed. An element size of 5 microns is considered in the contact region. The mesh refinement has been decreased gradually as moving away from the contact area. A two-dimensional, four nodes, plane strain element with full integration (CPE4) was used. A Coulomb friction model is employed for the contact between the pad and indenter using the Abaqus formulation for contact between two surfaces (master-slave) based on Lagrange multipliers. All the tests were performed under partial slip conditions. Thus, the COF is taken as 0.65.

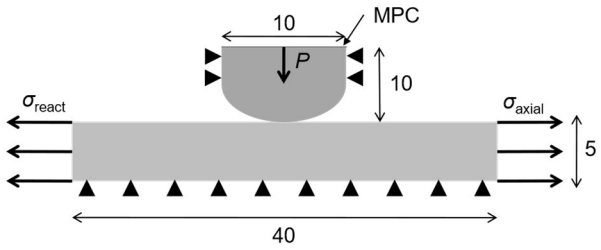


Figure 2: Sketch of the numerical model (dimensions in mm).

The fretting fatigue crack initiation has been numerically assessed by means of critical plane analysis using the well-known McDiarmid [29] (MD) and Smith-Watson-Topper [30] (SWT) criteria. The MD criterion is classified as a stress-based criterion. It predicts that the crack initiation will happen in the plane of maximum shear stress range ($\Delta\tau_{max}$). Between the two planes that reach the condition of $\Delta\tau_{max}$, the plane with the highest maximum normal stress ($\sigma_{n,max}$) is chosen. The MD equivalent stress can be calculated following Eq. 1, being $\Delta\tau_{f\text{-}1}$ the fatigue limit in torsion. The fatigue limit in torsion can be estimated dividing the uniaxial fatigue limit by $\sqrt{3}$ [10]. On the other hand, the SWT criterion is classified among the energy-based criteria. Under non-proportional loading, the criterion predicts that the crack initiation will happen in the plane normal to the orientation with maximum product of the amplitude of the first principal strain ($\Delta\varepsilon/2$) and first principal tensile stress ($\sigma_{max}$) (Eq. 2) [31]. Both criteria have been chosen to compare the results in the predicted cracks dominated by mode I (SWT) and mode II (MD). The predicted number of cycles to crack initiation ($N_{ini,pred}$) for MD and SWT criteria can be calculated in combination with the Basquin's equation as reported in Eq. 3 and Eq. 4, respectively [9]. The fatigue strength coefficient ($\sigma'_f$) and the fatigue strength exponent ($b$) are taken from [32], being 1194MPa and -0.133, respectively. These material constants are measured using smooth specimens. Although, Al2024-T3 has a low percentage of voids in comparison with other metals, such as those produced in castings or with metal additive manufacturing, voids can appear involuntarily as defects during

manufacturing or intentionally through perforation and acting as a possible palliative [24]. Furthermore, due to the lack of experimental data, the same fatigue constants are applied to assess the crack initiation lifetime at the hot-spots: the contact edges (surface) and voids (subsurface). However, the fatigue constants may change due to the different conditions (roughness, environment, etc…) found in the external surface and voids surfaces.

$$MD = \frac{\Delta\tau_{max}}{2} + \left(\frac{\Delta\tau_{f-1}}{2\sigma_u}\right)\sigma_{n,max} \quad (1)$$

$$SWT = \left(\sigma_{max}\frac{\Delta\epsilon}{2}\right)_{max} \quad (2)$$

$$MD = \frac{1}{2}\left(1 + \frac{\Delta\tau_{f-1}}{2\sigma_u}\right)\sigma'_f(2N_{ini,pred})^b \quad (3)$$

$$SWT = \frac{\sigma_f'^2}{E}(2N_{ini,pred})^{2b} \quad (4)$$

The area approach of the TCD [27] has been employed as well as the maximum approach. The maximum approach simply consists in calculating the initiation lifetime with the maximum value. However, in fretting fatigue, the stress field is not uniform at the vicinity of the contact edges and the components undergo a severe gradient. Thus, averaging methods over a process volume or area are employed to take into account the length scale of crack initiation and to reduce the dependence on the FEM solution [2]. The damage parameter has been averaged in a semi-circular region centred in the maximum value, perpendicular to the free surface (edge of the void and top surface of the specimen depending where is the maximum located) and with radius equal to $L/2$, where $L$ is the constant of Al-Haddad [33]. For Al2024-T3, the fatigue threshold stress intensity factor range for long cracks ($\Delta K_{th}$) is 1000MPa·mm$^{0.5}$[34] and the plain fatigue specimen strength ($\sigma_{0(10^6)}$) is 263MPa.

$$L = \frac{1}{\pi}\left(\frac{\Delta K_{th}}{\sigma_{0(10^6)}}\right) \quad (5)$$

The heterogeneity is included through the representation of micro-voids with circular shape. First, the specimen geometry (40×5mm) has been divided into cells of 2×1mm (100 cells). The cell distribution is shown in Fig 3. Furthermore, two distributions of voids are analysed: a) a regular distribution and b) a random distribution. In the regular distribution, the voids are equally spaced inside the cells and two void densities are analysed: a) 4 voids per cell (4 v.p.c.) and b) 1 void per cell (1 v.p.c.). In addition, 5 percentages of Void Surface (VS) are studied for both void densities by changing the void radius, i.e. 14%, 10%, 6%, 3.5% and 1.5%. These VS are in the range of the initial porosity fractions and are employed in similar studies found in the literature [35]. Table 3 tabulates all the VS studied with its corresponding void radius ($r_v$) for each void density. The FE models are generated through a Python script where all the void coordinates are introduced *a priori*. A further mesh refinement is employed around the voids belonging to the contacting cells, where the element size is 2 microns.

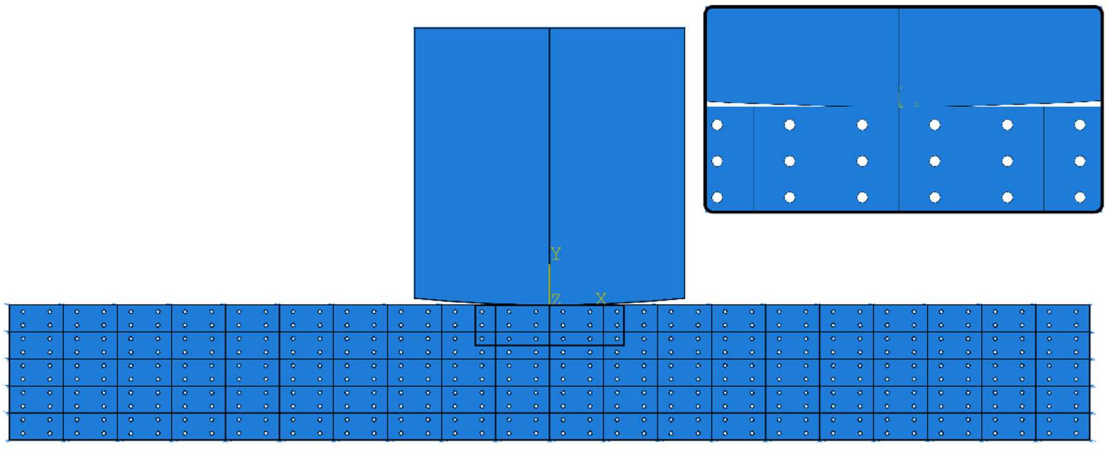

Figure 3: Geometry of the numerical model with 4 voids per cell and 3.5% of void surface.

| VS [%] | $r_v$ 1 v.p.c. [microns] | $r_v$ 4 v.p.c. [microns] |
|---|---|---|
| 14 | 300 | 150 |
| 10 | 250 | 130 |

| | | |
|---|---|---|
| 6 | 200 | 100 |
| 3.5 | 150 | 70 |
| 1.5 | 100 | 50 |

Table 3: Heterogeneous conditions studied and radius for both void surfaces (4 and 1 void per cell).

A random distribution is also considered because of the significant influence of the relative position between the micro-voids inside the cell [23]. Thus, twelve randomly distributed cases are studied with a VS of 1.5%. This VS and density of voids are chosen because the most realistic condition in aluminium alloys is considered among all the cases studied with regular distribution. The random distribution cases are created through a MatLab script developed to randomly generate the coordinates of the micro-voids considering two conditions: two voids cannot be overlapped, and a void cannot be on the edges. These conditions are imposed to ensure the convergence of the FE model. The twelve cases are shown in Fig. 4. For each case, the void distribution represented in Fig. 4 is repeated in each cell of the model. As in the normal distribution case, FE models are generated using a Python script. In a real application where pores or micro-voids are generated randomly, such as castings, these models are more realistic that the simple consideration of regularly distributed micro-voids. The generation of a random distribution of micro-voids will give further information about the influence of the micro-void positions.

## 3. Results and discussion

Numerical results are presented and discussed in this section. The section is divided taking into consideration whether the material is homogeneous, heterogeneous with a regular distribution of micro-voids or heterogeneous with a random distribution of micro-voids.

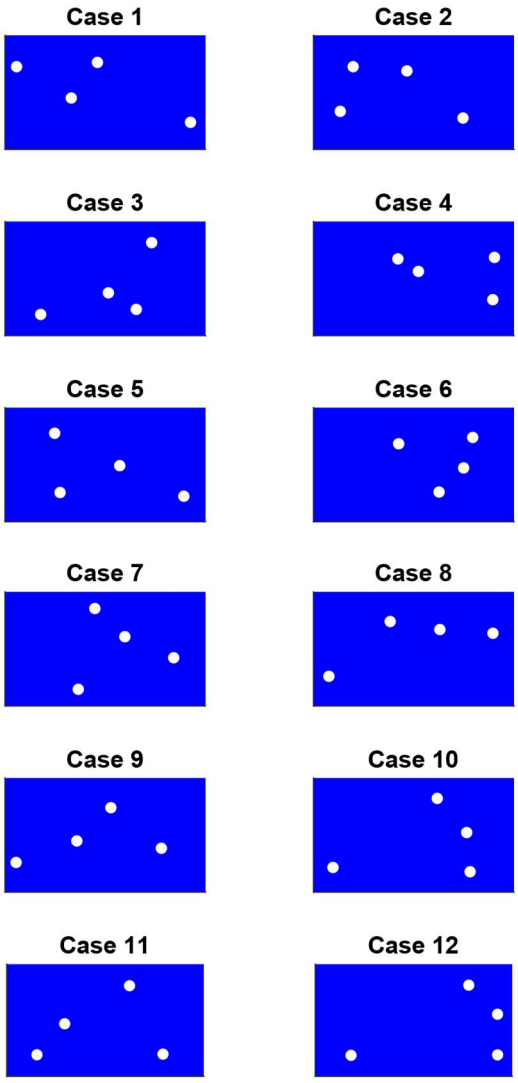


Figure 4: The twelve random void distributions in a cell studied in this work (cell size 2x1mm).

### 3.1. Homogeneous material

When the material is considered perfectly homogeneous, the problem is dominated by the stress concentration produced by the indenter around the contact edge [7]. Fig. 5 shows the fatigue damage map of SWT and MD in the specimen beneath the contact surface, circular markers in the figure represent the position of the end of the contact region. The damage is concentrated at the vicinity of the contact end as in the results obtained by Hojjati-Talemi et al. [7] and many other previous works found in the literature. Some

damage can be observed on the left contact edge, although the more critical region is clearly at the right contact edge. The location of the maximum SWT parameter (cross marker) is almost coincident with the contact edge while the maximum MD parameter is approximately located a few tens of microns from the contact edge inside the contact region. However, the location of the maximum MD parameter is more sensitive to the ratio between the tangential and axial load. As shown in Fig 5 b) and c), the maximum location moves towards the centre of the contact when the tangential load is increased under the same axial load. The same behaviour has been found when comparing the test conditions FF8 and FF9. On the other hand, it should be noted the high gradient found in both fatigue criteria damage maps, being more severe in the SWT criterion.

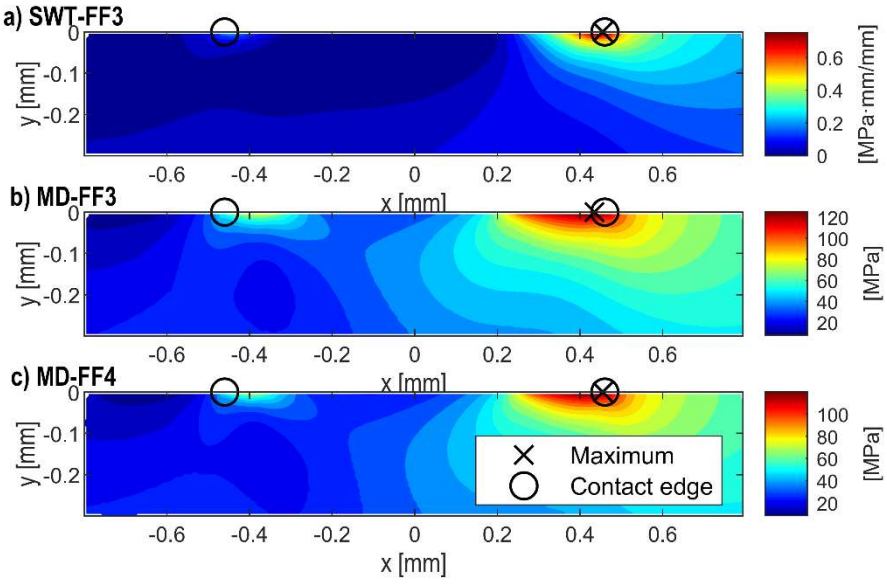


Figure 5: Colour damage map of a) SWT criterion and b) MD criterion for the FF3 test condition and c) MD criterion for the FF4 test condition in the region of the specimen just beneath the indenter.

The crack plane orientation predicted by the SWT and MD criteria are 95º and 45º (measured from the specimen top surface clockwise). The predicted crack plane orientation keeps constant for all the fretting conditions with a variation lower than 1º. The blue arrows of Fig. 6 show the predicted crack plane orientation in the centroid of the elements surrounding the right contact edge (circular marker). It is observed that the

plane orientation remains constant for both criteria. Hojjati-Talemi et al. reported in [7] an initial crack orientation of 130º after examining the fracture specimens. Thus, the crack orientation predicted by the SWT criterion is in better agreement than the MD prediction.

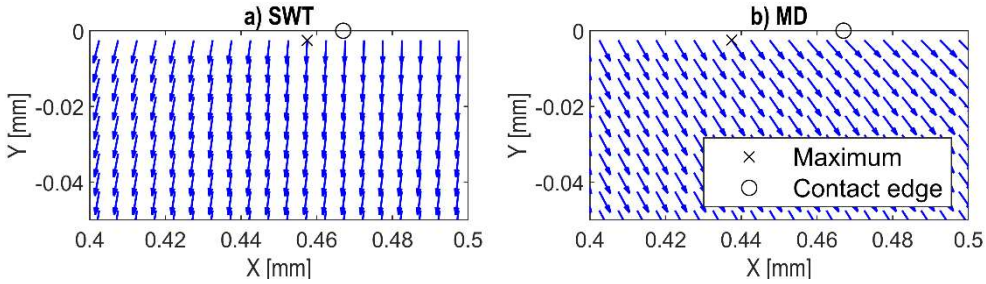


Figure 6: Predicted plane orientation (blue arrows) of a) SWT criterion and b) MD criterion for the FF1 loading case in the centroid of the elements located around the right contact edge (circular marker).

Lifetime prediction to crack initiation is performed using the maximum approach and area averaging approach of the TCD as explained in Section 2.2. Lifetime results of crack propagation are taken from [6], where crack propagation lifetime is calculated using FEM and LEFM from an initial planar crack of 50 microns (further details in [6]). Fig. 7 shows the lifetime prediction to total fracture for the 9 conditions tested with both approaches and damage parameters. It can be shown that both approaches and damage criteria predict less conservative results at low loads (longer lives) as shown in Fig. 7. The maximum approach gives more conservative results and little difference can be found between both damage criteria. In order to compare the accuracy and dispersion of the predicted results, a quantitative study is presented in Table 4 following the methodology proposed by Navarro et al. in [9]. The dispersion (SD) and mean ratio ($\bar{x}$) are presented using a logarithm scale. The following equations are employed ($i$ represents each test condition and $N$ is the total number of tested conditions):

$$\bar{\alpha} = \frac{1}{N}\sum_{i=1}^{N} \log \frac{N_{f\,i}}{N_{predicted\,i}} \tag{6}$$

$$SD_\alpha = \sqrt{\frac{N}{N-1}\sum_{i=1}^{N}\left(\log\frac{N_{f\,i}}{N_{predicted\,i}} - \bar{\alpha}\right)^2} \tag{7}$$

$$\bar{x} = 10^{\bar{\alpha}} \tag{8}$$

$$SD = 10^{SD_\alpha} \tag{9}$$

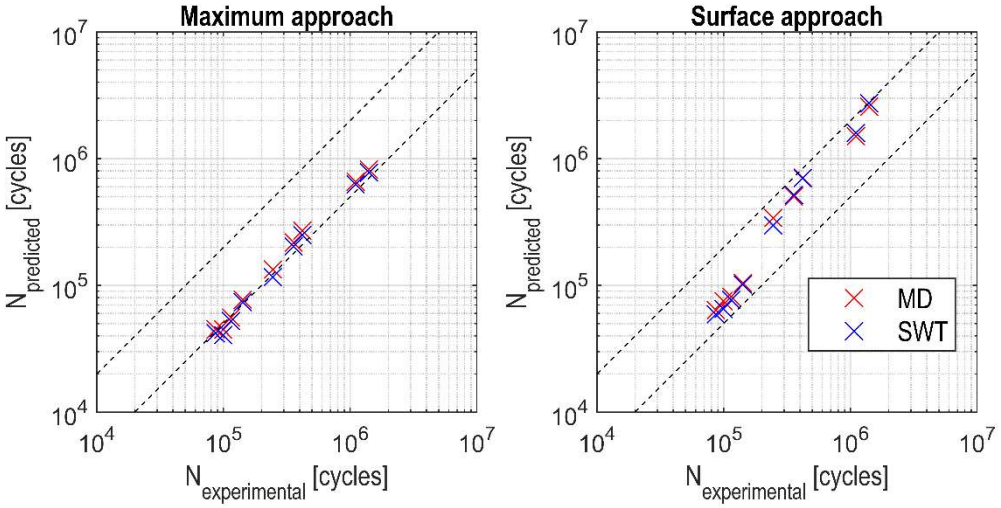


Figure 7: Predicted and experimental results of total lifetime with the maximum approach (left) and area approach (right), dashed lines indicate scatter bands of ±2N.

A good prediction results in a mean ratio close to 1. As expected, the maximum approach gives more conservative results (see Table 4). The predicted results obtained with the criterion of MD and SWT using the area approach are within the scatter bands (dashed lines) with factor equal to 2. A better agreement is obtained with the SWT criterion, whereas a lower deviation of the results is obtained for the MD criterion. The differences between experimental and predicted results may be due to the scatter in the experimental data. However, the predictions are acceptable as concluded in similar works [36,37].

| | McDiarmid | | Smith Watson Topper | |
|---|---|---|---|---|
| | $\bar{x}$ | SD | $\bar{x}$ | SD |
| **Maximum approach** | 1.82 | 1.12 | 1.96 | 1.13 |
| **Area approach** | 0.90 | 1.49 | 0.94 | 1.56 |

Table 4: Statistical quantitative comparison of the predicted and experimental cycles to total fracture.

### 3.2. Normal distribution of micro-voids

When the material is considered heterogeneous in the numerical model, there is a competition of crack initiation between the stress concentration produced at the right contact edge and at the neighbouring micro-voids. The introduction of the micro-voids changes the contact stress distribution between indenter and specimen [23], and therefore it completely changes the mechanics of the problem. Thus, it is expected that the predicted results in crack initiation will be affected as well.

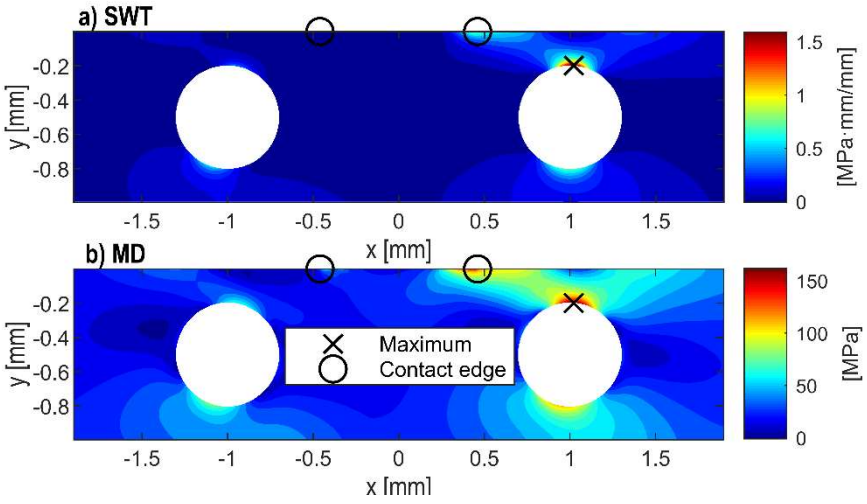


Figure 8: Colour damage map of SWT (top) and MD (bottom) parameters on the two cells located just beneath the indenter for the FF1 test condition, 1 v.p.c. and 14% VS.

The damage map for MD and SWT criteria with different VS and density for FF1 loading conditions are presented in Fig. 8 to Fig. 11. These figures contain the damage map information of the two cells just beneath the indenter (circular marks represent the end of

the contact zone). When the VS is higher than 1.5%, the location of the maximum value changes from the contact edge to the upper edge of the micro-void as shown in Fig. 10 and in Fig. 11.

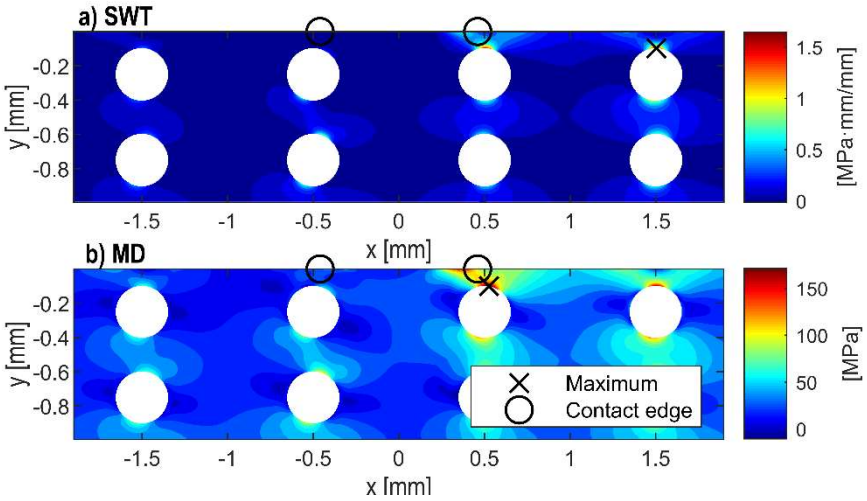


Figure 9: Colour damage map of SWT (top) and MD (bottom) parameters on the two cells located just beneath the indenter for the FF1 test condition, 4 v.p.c. and 14% VS.

Furthermore, the maximum location of SWT and MD does not coincide in some cases, changing from different micro-voids (see Fig. 9) or from the contact edge to the micro-void as shown in Fig. 11. In some cases, the maximum global damage point is located at the micro-void upper edge, but the damage gradient is lower at the fretting contact edge (see Fig. 11).

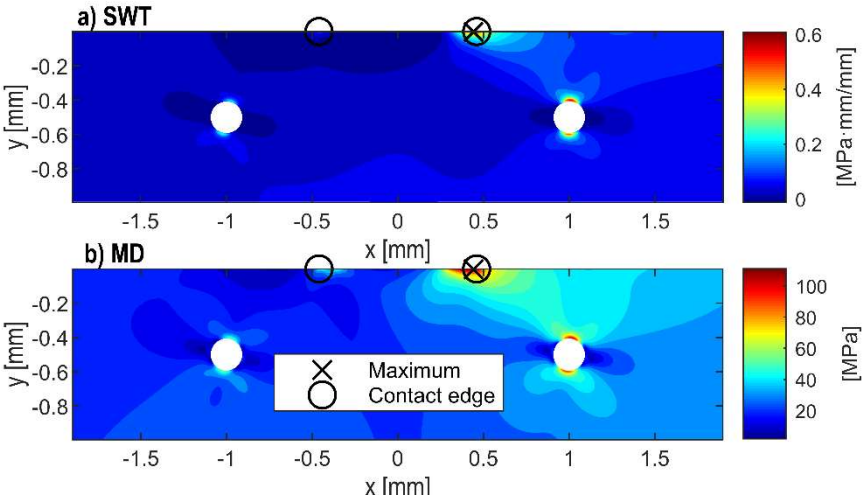


Figure 10: Colour damage map of SWT (top) and MD (bottom) parameters on the two cells located just beneath the indenter for the FF1 test condition, 1 v.p.c. and 1.5% VS.

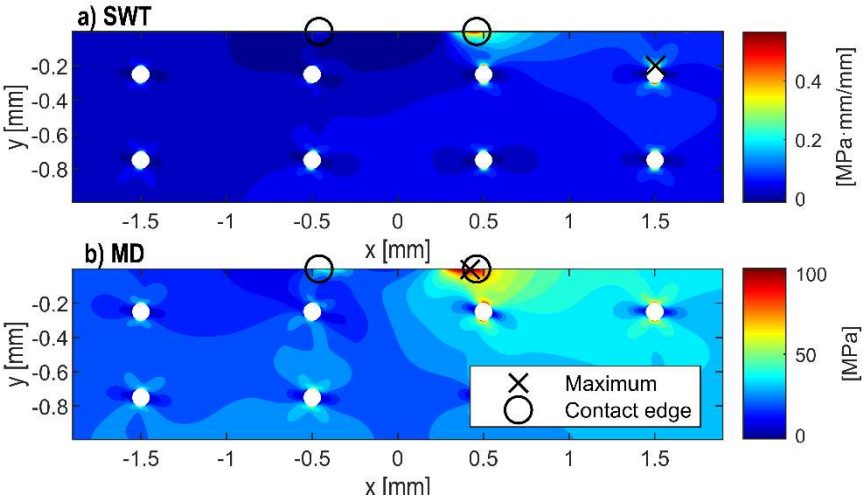


Figure 11: Colour damage map of a) SWT criterion and b) MD criterion on the two cells located just beneath the indenter for the FF1 test condition, 4 v.p.c. and 1.5% VS.

As the location of the maximum value in the damage parameters is changing, the crack may initiate first at the micro-void edge or at the contact edge. In some cases, multiple cracks are predicted to initiate simultaneously at both spots. The area approach is employed to predict the crack initiation lifetime at the local maximum near the two spots: the fretting contact edge and the micro-void. Figs. 12 and 13 show the normalized values of the fretting fatigue initiation lives predicted with the MD and SWT for the FF1 loading case with 1 and 4 voids per cell. Each value is normalized to the predicted initiation

lifetime with the same damage parameter obtained for the homogeneous case with the same effective section. In other words, the introduction of micro-voids will directly produce a reduction of the net section of the specimen and, thus, it will increase the nominal axial stress and obviously reduce the crack initiation lifetime. In order to isolate the effect of the micro-voids introduction, the predicted initiation lives employed in the homogeneous case for the normalization has been calculated using a maximum axial stress corresponding to the same effective section. In this way, it can be compared directly the reduction or increment in the initiation lifetime when considering the material heterogeneous in the numerical model. The initiation lifetime is calculated at the local maximum near the fretting contact edge and the micro-void. In the regular distribution with 1 v.p.c., the predicted crack initiation lifetime at the contact edge spot is lower than in the homogeneous case for all the studied cases. In addition, the numerical model predicts that the crack grows firstly in the micro-void when the VS is lower than 3.5%. The lifetime predicted by the MD criterion is usually higher than the one predicted by the SWT at the micro-void and contact edge hot-spot.

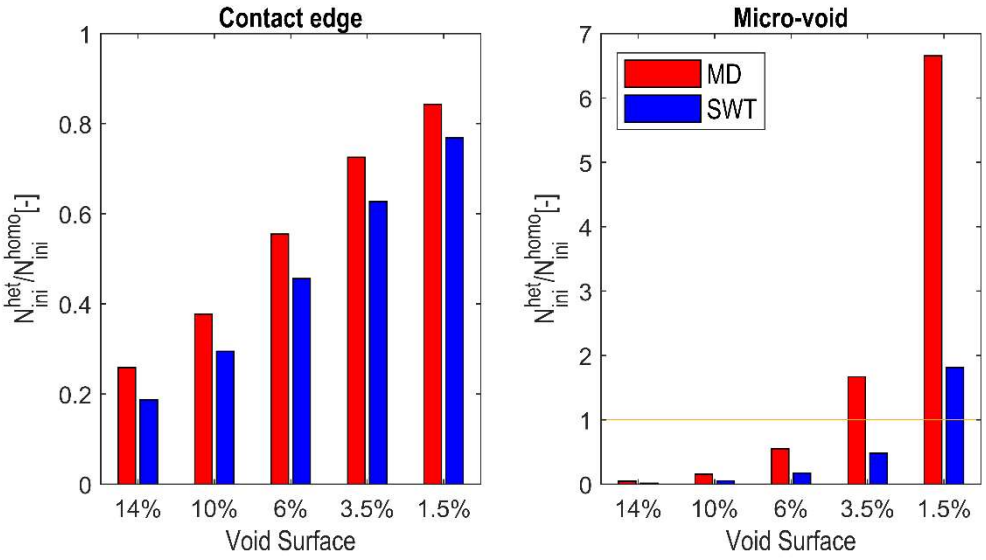


Figure 12: Bar charts of the predicted normalized lives for initiation with the MD and SWT criteria for the FF1 loading case with 1 void per cell calculated at the contact edge and micro-void.

As shown in Fig. 13, the predicted lifetime at the contact edge spot by the MD criterion is lower than the predicted by the SWT, contrary to the 1 v.p.c. case. In addition, the crack initiation is predicted to start at the micro-void spot for VS higher than 6%. On the other hand, it is shown that the predicted lifetime by the SWT criterion is not affected at the contact edge spot for VS lower than 3.5%. This effect will be further described in the random distribution. In the case of regular distribution of 1 v.p.c., voids have a larger radius than in the 4 v.p.c. case for the same VS, but they are located at a larger distance to the contact edge in the *y* and *x* axis. Further, it must be noted that as decreasing the size of micro-voids, the upper edge of the micro-void moves away from the contact edge although the effective strength section is increasing. When comparing the results obtained between the two regular distributions, it can be concluded that the position of the micro-voids has a significant influence in the lifetime prediction as well as its relative size to the right contact edge.

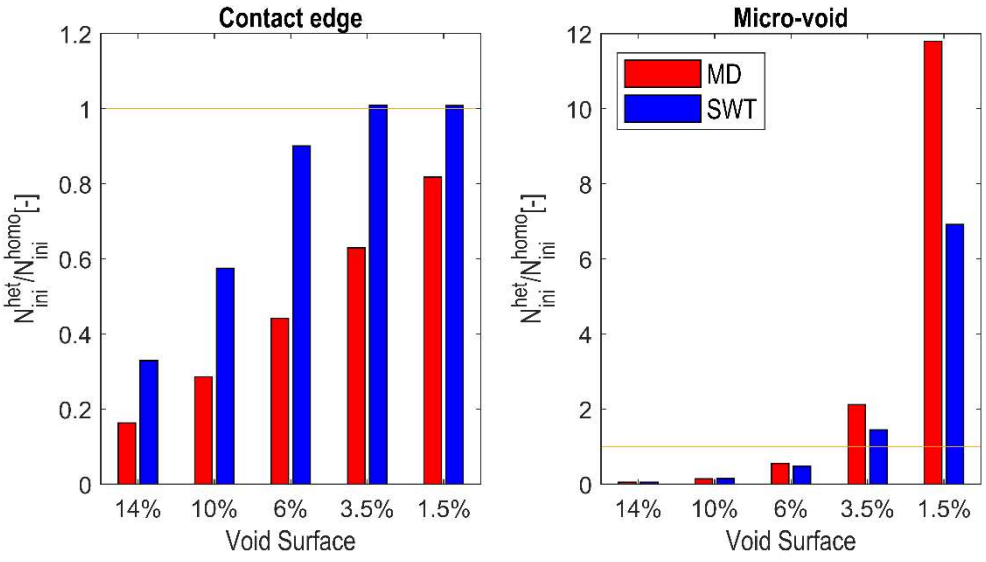


Figure 13: Bar charts of the predicted normalized lives for initiation with the MD and SWT criteria for the FF1 loading case with 4 voids per cell calculated at the contact edge and micro-void.

### 3.3. Random distribution of micro-voids

As commented in the previous section, the micro-void distribution plays a crucial role in the predicted initiation life. Furthermore, materials usually show a random distribution of micro-voids. For these reasons, the study of a random distribution is a must to obtain more realistic conclusions. The results shown in this section are obtained using a random distribution of 4 v.p.c. with 1.5% of VS. This case is selected as the most realistic one between the studied cases in the regular distribution because it has the lower micro-void radius. Fig. 14 shows the damage map obtained for the case 1 of the random distribution and FF1 loading condition. It is observed again that the SWT criterion predicts its maximum at the upper micro-void edge, but the MD criterion does not. It has been observed in all cases that the maximum of both damage criteria is always predicted at the right contact edge when the micro-void is at a distance higher than 0.4mm from the right contact edge for both criteria. In addition, micro-voids located at the right side of the right contact edge are potentially more dangerous for both crack initiation criteria, because as shown in the damage map of the homogeneous case (see Fig 5), the right side of the right contact edge shows a higher intensity of the damage field.

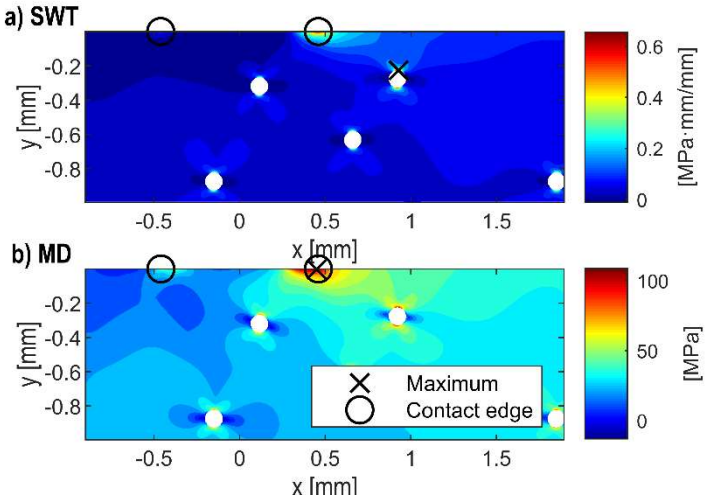


Figure 14: Colour damage map of a) SWT criterion and b) MD criterion on the specimen located just beneath indenter for the case 1 of the random distribution and FF1 loading condition.

Fig. 15 shows the predicted lives for the 12 random distributions and FF1 loading case at the contact edge and micro-void spots. Initiation lifetimes are shown normalized to the initiation lifetime predicted for the homogeneous case as well as for the regular distribution. The high scattering of the predicted initiation lifetime at the micro-voids is observed. Only two cases have been found that crack will firstly start at the micro void. In addition, the micro-void needs to be very close (below 0.4 mm distance) to the right contact edge. In this way, it is expected that both crack initiate at the same time. Yi et al. [25] observed experimentally a high scattering in the plain fatigue life of a porous aluminium. Further, they also observed that large pores located near the specimen surface were responsible for crack initiation. Our results are in line with the conclusions obtained by Yi et al. [25] under plain fatigue. However, under fretting fatigue conditions, the stress concentration produced at the vicinity of the contact edge dominates the damage initiation. In the numerical model, only micro-voids located very close to the contact edge will decrease the initiation lifetime. On the other hand, it is observed a mean reduction of 3% and 9% in the predicted initiation lifetime for the MD and SWT criterion, respectively. The predicted lives at the fretting contact edge by the MD criterion are higher than the predicted with the SWT criterion.

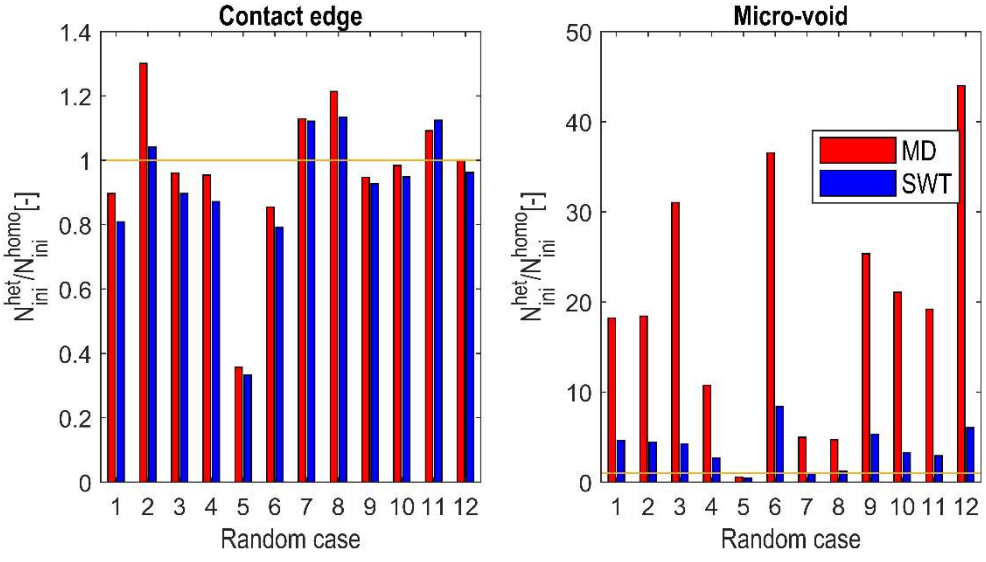

Figure 15: Bar charts of the predicted normalized lives for initiation with the MD and SWT criteria for the FF1 loading case with random distribution 4 calculated at the contact edge and micro-void.

Four cases can be observed (cases 2, 7, 8 and 11) for which the predicted life by the SWT criterion at the contact edge is higher than in the homogeneous case. The reason of this increase in the predicted lifetime is due to their singular micro-void distribution, slightly decreasing the stiffness of the component at the right side of the contact area. Therefore, increasing the contact area and decreasing the stress intensity at that region. Fig. 16 shows the contact pressure distribution along the contact area between the indenter and specimen for the homogeneous case and the random distribution case 2. The contact pressure distribution is almost identical on the left side of the contact. However, a small variation can be observed on the right side. This slight change in the contact pressure distribution is due to the loss of stiffness caused by the particular micro-void distribution and results in the increase of the crack initiation lifetime. This result is in line with the results obtained by Erena et al. [24], where the introduction of voids beneath the contact surface in a fretting wear numerical model decreases the damage severity for crack initiation. Nevertheless, further experimental tests should be performed to obtain firmer conclusions.

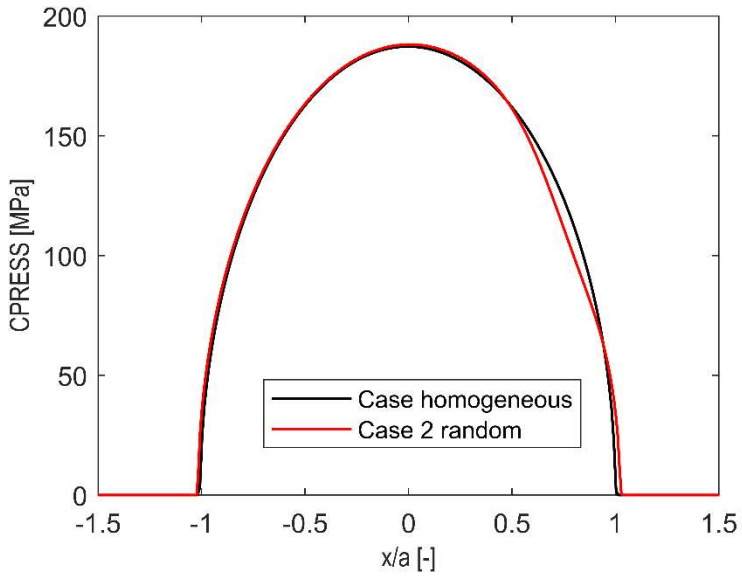

Figure 16: Contact pressure along the contact area for the homogeneous case and case 2 of the random distribution.

.

## 4. Conclusions

In this work, a numerical analysis has been performed in a homogeneous and heterogeneous material to compare the results in terms of the predicted initiation lifetime. A critical plane analysis with the McDiarmid and Smith-Watson-Topper criteria in combination with the theory of critical distances has been employed to assess the initiation lifetime. The main conclusions obtained are:

1. The location predicted in the homogeneous material by MD and SWT criteria is at the right edge of the contact. In some cases, the location changes to beneath the indenter for high tangential loads.
2. A better agreement with the experimental results has been obtained with the SWT criterion in terms of initiation lifetime. In addition, the crack orientation reported by Hojjati-Talemi et al. [7] is more in concordance with the results obtained with the SWT criterion.
3. Predicted crack initiation lifetime usually decreases when the material has been considered heterogeneous with regular distribution for severe void surface percentage. However, a large scattering in the predicted lifetime has been obtained for the studied random distributions, in some cases leading to an increase of the predicted fretting fatigue lifetime by MD and SWT criteria.
4. The numerical model shows that a crack may initiate firstly at the micro-voids located close to the right contact edge. However, it has been shown that the stress concentration produced by the fretting contact edge dominates the crack initiation since cracks need to be very close to it. The initiation lifetime predicted by the

SWT criterion is lower than the initiation lifetime predicted by the MD at the micro-void hot-spot.

5. In the following order of severity, size, distribution and density of micro-voids have shown a significant influence on the predicted initiation lifetime compared to the predicted results in the homogeneous case.

Future work will seek the 3D modelling and the study of different micro-void shapes. The 2D problem simplification adequately models the plane-to-cylinder contact configuration, but the presence of micro-voids will generally produce a 3D variation of the flow stress due to the material discontinuities. In addition, the shape of micro-voids is also a significant parameter to be considered. However, this research represents a starting point to analyse the effect of micro-voids before performing a 3D analysis. Finally, more experimental validation will be fundamental to draw firmer conclusions. These tests may involve specimens made by metal additive manufacturing.

## 5. Acknowledgements

The authors gratefully acknowledge the financial support given by the Spanish Ministry of Economy and Competitiveness and the FEDER program through the projects DPI2017-89197-C2-1-R, DPI2017-89197-C2-2-R and the FPI subprogram with the reference BES-2015-072070. The support of the Generalitat Valenciana, Programme PROMETEO 2016/007, is also acknowledged.

The last author would like to acknowledge the financial support of the Research Foundation-Flanders (FWO), The Luxembourg National Research Fund (FNR) and Slovenian Research Agency (ARRS) in the framework of the FWO Lead Agency project: G018916N 'Multi-analysis of fretting fatigue using physical and virtual experiments'.

## References

[1] Hills DA, Nowell D. Mechanics of fretting fatigue-Oxford's contribution. Tribol Int 2013;76:1–5. doi:10.1016/j.triboint.2013.09.015.

[2] Hojjati-Talemi R, Wahab MA, Giner E, Sabsabi M. Numerical estimation of fretting fatigue lifetime using damage and fracture mechanics. Tribol Lett 2013;52:11–25. doi:10.1007/s11249-013-0189-8.

[3] Nowell D, Dini D, Hills DA. Recent developments in the understanding of fretting fatigue. Eng Fract Mech 2006;73:207–22. doi:10.1016/j.engfracmech.2005.01.013.

[4] Amargier R, Fouvry S, Chambon L, Schwob C, Poupon C. Stress gradient effect on crack initiation in fretting using a multiaxial fatigue framework. Int J Fatigue 2010;32:1904–12. doi:10.1016/j.ijfatigue.2010.06.004.

[5] Proudhon H, Fouvry S, Buffière JY. A fretting crack initiation prediction taking into account the surface roughness and the crack nucleation process volume. Int J Fatigue 2005;27:569–79. doi:10.1016/j.ijfatigue.2004.09.001.

[6] Pereira K, Abdel Wahab M. Fretting fatigue crack propagation lifetime prediction in cylindrical contact using an extended MTS criterion for non-proportional loading. Tribol Int 2017;115:525–34. doi:10.1016/J.TRIBOINT.2017.06.026.

[7] Hojjati-Talemi R, Abdel Wahab M, De Pauw J, De Baets P. Prediction of fretting fatigue crack initiation and propagation lifetime for cylindrical contact configuration. Tribol Int 2014;76:73–91. doi:10.1016/J.TRIBOINT.2014.02.017.

[8] Noraphaiphipaksa N, Manonukul A, Kanchanomai C, Noraphaiphipaksa N, Manonukul A, Kanchanomai C. Fretting Fatigue with Cylindrical-On-Flat Contact: Crack Nucleation, Crack Path and Fatigue Life. Materials (Basel) 2017;10:155. doi:10.3390/ma10020155.

[9] Navarro C, Muñoz S, Domínguez J. On the use of multiaxial fatigue criteria for

fretting fatigue life assessment. Int J Fatigue 2008;30:32–44. doi:10.1016/J.IJFATIGUE.2007.02.018.

[10] Bhatti NA, Abdel Wahab M. A numerical investigation on critical plane orientation and initiation lifetimes in fretting fatigue under out of phase loading conditions. Tribol Int 2017;115:307–18. doi:10.1016/j.triboint.2017.05.036.

[11] Sabsabi M, Giner E, Fuenmayor FJ. Experimental fatigue testing of a fretting complete contact and numerical life correlation using X-FEM. Int J Fatigue 2011;33:811–22. doi:10.1016/J.IJFATIGUE.2010.12.012.

[12] Szolwinski MP, Farris TN. Observation, analysis and prediction of fretting fatigue in 2024-T351 aluminum alloy. Wear 1998;221:24–36. doi:10.1016/S0043-1648(98)00264-6.

[13] Lu L, Nogita K, McDonald SD, Dahle AK. Eutectic solidification and its role in casting porosity formation. Jom 2004;56:52–8. doi:10.1007/s11837-004-0254-8.

[14] Gong H, Rafi K, Gu H, Starr T, Stucker B. Analysis of defect generation in Ti–6Al–4V parts made using powder bed fusion additive manufacturing processes. Addit Manuf 2014;1–4:87–98. doi:10.1016/J.ADDMA.2014.08.002.

[15] Rajasekaran B, Ganesh Sundara Raman S, Joshi S V., Sundararajan G. Effect of grinding on plain fatigue and fretting fatigue behaviour of detonation gun sprayed Cu-Ni-In coating on Al-Mg-Si alloy. Int J Fatigue 2009;31:791–6. doi:10.1016/j.ijfatigue.2008.03.003.

[16] Chan LC, Lu XZ, Yu KM. Multiscale approach with RSM for stress-strain behaviour prediction of micro-void-considered metal alloy. Mater Des 2015;83:129–37. doi:10.1016/j.matdes.2015.05.064.

[17] Forsyth P. No Title. Proc Crack Propag Symp Coll Aeronaut 1961;1:76–94.

[18] Dubourg M, Lamacq V. Stage II crack propagation direction determination under

fretting fatigue loading: a new approach in accordance with experimental observations. Frett. Fatigue Curr. Technol. Pract., 100 Barr Harbor Drive, PO Box C700, West Conshohocken, PA 19428-2959: ASTM International; 2000, p. 436-436–15. doi:10.1520/STP14746S.

[19] Bhatti NA, Abdel Wahab M. Fretting fatigue crack nucleation: A review. Tribol Int 2018;121:121–38. doi:10.1016/j.triboint.2018.01.029.

[20] Marco M, Infante-García D, Díaz-Álvarez J, Giner E. Relevant factors affecting the direction of crack propagation in complete contact problems under fretting fatigue. Tribol Int 2019;131:343–52. doi:10.1016/j.triboint.2018.10.048.

[21] Muñoz S, Navarro C, Domínguez J. Application of fracture mechanics to estimate fretting fatigue endurance curves. Eng Fract Mech 2007;74:2168–86. doi:10.1016/J.ENGFRACMECH.2006.10.010.

[22] Giner E, Sabsabi M, Ródenas JJ, Javier Fuenmayor F. Direction of crack propagation in a complete contact fretting-fatigue problem. Int J Fatigue 2014;58:172–80. doi:10.1016/j.ijfatigue.2013.03.001.

[23] Kumar D, Biswas R, Poh LH, Wahab MA. Fretting fatigue stress analysis in heterogeneous material using direct numerical simulations in solid mechanics. Tribol Int 2017;109:124–32. doi:10.1016/j.triboint.2016.12.033.

[24] Erena D, Vázquez J, Navarro C, Domínguez J. Voids as stress relievers and a palliative in fretting. Fatigue Fract Eng Mater Struct 2018;41:2475–84. doi:10.1111/ffe.12849.

[25] Buffière J-Y, Savelli S, Jouneau PH, Maire E, Fougères R. Experimental study of porosity and its relation to fatigue mechanisms of model Al–Si7–Mg0.3 cast Al alloys. Mater Sci Eng A 2001;316:115–26. doi:10.1016/S0921-5093(01)01225-4.

[26] Mayer H, Papakyriacou M, Zettl B, Stanzl-Tschegg S. Influence of porosity on

the fatigue limit of die cast magnesium and aluminium alloys. Int J Fatigue 2003;25:245–56. doi:10.1016/S0142-1123(02)00054-3.

[27] Taylor D. The theory of critical distances. Eng Fract Mech 2008;75:1696–705. doi:10.1016/J.ENGFRACMECH.2007.04.007.

[28] Araújo J., Nowell D. The effect of rapidly varying contact stress fields on fretting fatigue. Int J Fatigue 2002;24:763–75. doi:10.1016/S0142-1123(01)00191-8.

[29] McDiarmid DL. A GENERAL CRITERION FOR HIGH CYCLE MULTIAXIAL FATIGUE FAILURE. Fatigue Fract Eng Mater Struct 1991;14:429–53. doi:10.1111/j.1460-2695.1991.tb00673.x.

[30] Smith K, Watson T, Topper. A stress-strain function for the fatigue of metals. J Mater 1970;5:767–78.

[31] Socie D. Multiaxial Fatigue Damage Models. J Eng Mater Technol 1987;109:293. doi:10.1115/1.3225980.

[32] Gates N, Fatemi A. Multiaxial variable amplitude fatigue life analysis including notch effects. Int J Fatigue 2016;91:337–51. doi:10.1016/J.IJFATIGUE.2015.12.011.

[33] El Haddad MH, Dowling NE, Topper TH, Smith KN. J integral applications for short fatigue cracks at notches. Int J Fract 1980;16:15–30. doi:10.1007/BF00042383.

[34] Forman RG, Shivakumar V, Cardinal JW, Williams LC, McKeighan PC. Fatigue crack growth database for damage tolerance analysis. 2005.

[35] Kim J, Gao X, Srivatsan TS. Modeling of void growth in ductile solids: effects of stress triaxiality and initial porosity. Eng Fract Mech 2004;71:379–400. doi:10.1016/S0013-7944(03)00114-0.

[36] Fatemi A, Socie DF. A critical plane approach to multiaxial fatigue damage

including out-of-phase loading. Fatigue Fract Eng Mater Struct 1988;11:149–65. doi:10.1111/j.1460-2695.1988.tb01169.x.

[37] Lykins CD, Mall S, Jain VK. Combined experimental–numerical investigation of fretting fatigue crack initiation. Int J Fatigue 2001;23:703–11. doi:10.1016/S0142-1123(01)00029-9.